Lithos 218-219 (2015) 117–126

Contents lists available at ScienceDirect

Lithos

journal homepage: www.elsevier.com/locate/lithos

Geochemistry and petrogenesis of volcanic rocks from Daimao Seamount (South China Sea) and their tectonic implications

Quanshu Yan [a], Paterno Castillo [b], Xuefa Shi [a,*], Liaoliang Wang [c], Lin Liao [c], Jiangbo Ren [c]

[a] Key Laboratory of Marine Sedimentary and Environmental Geology, The First Institute of Oceanography, State Oceanic Administration, Qingdao, 266061, PR China
[b] Scripps Institution of Oceanography, UCSD, La Jolla, CA 92093, USA
[c] Guangzhou Marine Geological Survey, Guangzhou, 510760, PR China

ARTICLE INFO

Article history:
Received 26 June 2014
Accepted 31 December 2014
Available online 13 January 2015

Keywords:
Geochemistry
Tectonic evolution
Mantle source
South China Sea
Daimao Seamount

ABSTRACT

The South China Sea (SCS) experienced three episodes of seafloor spreading and left three fossil spreading centers presently located at 18°N, 17°N and 15.5°N. Spreading ceased at these three locations during magnetic anomaly 10, 8, and 5c, respectively. Daimao Seamount (16.6 Ma) was formed 10 my after the cessation of the 17°N spreading center. Volcaniclastic rocks and shallow-water carbonate facies near the summit of Daimao Seamount provide key information on the seamount's geologic history. New major and trace element and Sr–Nd–Pb isotopic compositions of basaltic breccia clasts in the volcaniclastics suggest that Daimao and other SCS seamounts have typical ocean island basalt-like composition and possess a 'Dupal' isotopic signature. Our new analyses, combined with available data, indicate that the basaltic foundation of Daimao Seamount was formed through subaqueous explosive volcanic eruptions at 16.6 Ma. The seamount subsided rapidly (>0.12 mm/y) at first, allowing the deposition of shallow-water, coral-bearing carbonates around its summit and, then, at a slower rate (<0.12 mm/y). We propose that the parental magmas of SCS seamount lavas originated from the Hainan mantle plume. In contrast, lavas from contemporaneous seamounts in other marginal basins in the western Pacific are subduction-related.

1. Introduction

The origins of marginal or backarc basins in the western Pacific and the many features of these basins are still poorly understood (Hall, 2002; Karig, 1971). For example, volcanic seamounts near fossil spreading centers are common in the Oligocene to Miocene South China Sea (SCS), Shikoku and Sea of Japan basins, but their origin and geodynamic importance are still debated (e.g., Ishizuka et al., 2009; Tu et al., 1992; Yan et al., 2008a, b, 2014). In the Shikoku and Sea of Japan basins, seamounts were formed immediately after the cessation of seafloor spreading (e.g., Ishizuka et al., 2009; Kaneoka et al., 1990; Klein et al., 1978; Pouclet et al., 1995). In the SCS, however, three fossil spreading centers and a number of seamounts were formed ~6–12 my after the cessation of spreading (Briais et al., 1993; Yan et al., 2008b). Studies on their petrogenesis and geodynamic significance have been limited because of the dearth of samples and the fact that these had been dredged from relatively imprecise locations (e.g., Shi and Yan, 2011; Tu et al., 1992; Wang et al., 1984; Yan et al., 2008a, b, 2014).

Here we present new observations as well as major-trace element and Sr–Nd–Pb isotopic analyses of individual basaltic lava breccias as well as bulk volcaniclastic rocks. These rocks have recently been sampled *in situ* from Daimao Seamount through shallow core drilling by *R/V Ocean No. 6*, Guangzhou Marine Geological Survey, Ministry of Land and Resources of the People's Republic of China. We combined our new analyses with available geochemical data for samples previously dredged from SCS seamounts and geophysical data for the SCS to constrain the origin and evolution of Daimao and other seamounts in the SCS. Our results are highly consistent with the recently proposed regional tectonic evolution of the SCS region (Yan et al., 2014).

2. Geological setting and sample description

The SCS is one of the largest marginal basins in the western Pacific (Fig. 1). It was formed by the southeastward rifting of several microcontinental blocks and subsequent seafloor spreading from ~37 Ma to ~16 Ma (Briais et al., 1993; Cande and Kent, 1995; Hsu et al., 2004). During the Cenozoic, the SCS underwent three episodes of seafloor spreading (Briais et al., 1993). Spreading ceased at present day 18°N (magnetic anomaly 10) in the northwest sub-basin and commenced at present day 17°N (magnetic anomaly 8) in the east sub-basin at ~30 Ma. Spreading ceased again at 17°N and commenced at present day 15.5°N in the east sub-basin and in the southwest sub-basin at ~26–24 Ma. Spreading finally stopped at 16 Ma (magnetic anomaly 5c) (Cande and Kent, 1995; Hsu et al., 2004), leaving three fossil spreading centers within the basin (Fig. 1).

* Corresponding author.
E-mail addresses: yanquanshu@163.com (Q. Yan), shixuefa@163.com (X. Shi).

http://dx.doi.org/10.1016/j.lithos.2014.12.023
0024-4937/

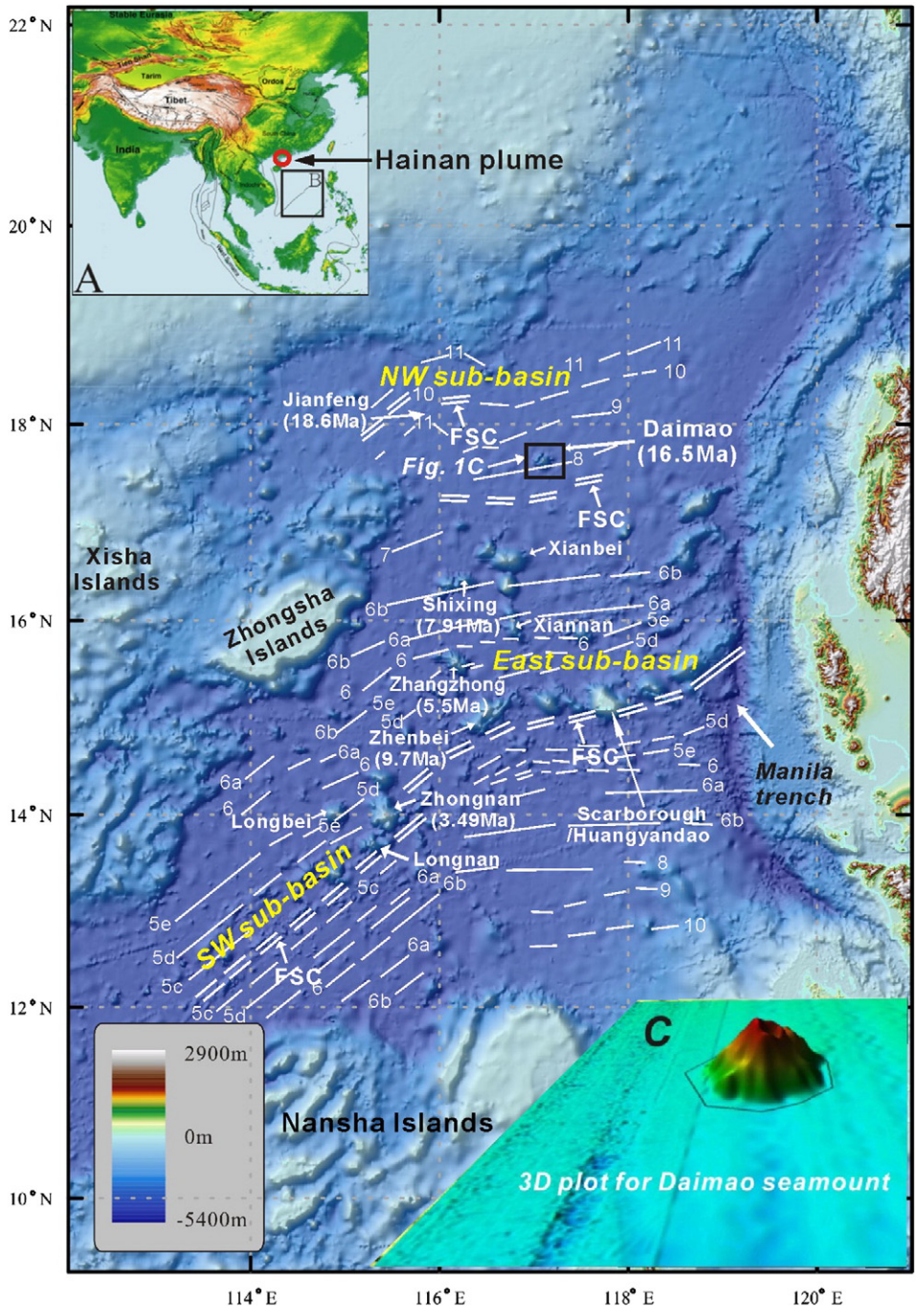

Fig. 1. (A) Tectonic location of the SCS, and (B) geological map of the South China Sea (SCS) and drilling location in Daimao Seamount. The magnetic anomaly lines are gray lines and spreading axes are white double lines. There are three fossil spreading centers: the first one is oriented E–W in the northwest (NW) sub-basin; the second one is oriented E–W in the east sub-basin (near the present 17°N); and the third one is also in the east sub-basin (15.5°N) but extends southwestward into the southwest (SW) sub-basin. Data are from Briais et al. (1993). The ages of seamounts obtained by previous dating investigations (Yan et al., 2008b) are also shown. (C) 3-D plot of Daimao Seamount.

In addition to seafloor spreading magmatism, within plate magmatism is also associated with the history of the SCS basin. Prior to Cenozoic spreading (60–43 Ma or 32 Ma), bimodal volcanics formed along the northern margin of the SCS (e.g., Chung et al., 1997; Zhou et al., 2009). After the cessation of spreading, intraplate volcanism occurred around the SCS (e.g., Pearl River Mouth Basin, Leiqiong Peninsula, Beibu Gulf, Indochina block — Flower et al., 1992; Hoang and Flower, 1998; Lee et al., 1998; K.L. Wang et al., 2012; X.-C. Wang et al., 2012; Zhou and Mukasa, 1997; Zou and Fan, 2010; Zou et al., 1995; along the coastal areas of the Fujian Province — Ho et al., 2003; Zou et al., 2000, 2004), near and/or along the 15.5°N fossil spreading center (Tu et al., 1992; Yan et al., 2008a), and in Nansha islands (Kudrass et al., 1986). Based on a limited amount of age data (Wang et al., 1984; Yan et al., 2014), the seamounts generally show a younging trend from the northwest sub-basin to the Scarborough (Huangyandao in Chinese) seamount chain, approximately corresponding to the age of the underlying oceanic crust (inferred from magnetic anomalies; Fig. 1B). Consequently, the igneous rocks from SCS seamounts and volcanoes in the surrounding areas contain a record of the source and evolution of intraplate or post-spreading volcanism that commenced as early as ~18 Ma and still is currently active at the northern margin of the SCS and in the Indochina block.

Daimao Seamount is located near the 17°N fossil spreading center between the east and northwest sub-basins (Fig. 1) and was formed at 16.6 Ma (Table 1). It occupies an area of ~1400 km^2; its radius

Table 1
Major and trace element compositions of the volcaniclastic rocks and basaltic breccias from Daimao Seamount, SCS.

Location	Daimao seamount (117°05.1′E, 17°38.9′N, 2300 m water depth)													
Samples No.	BBL	VC-1	VC-1-1*	VC-2	VC-3	VC-4	VC-5	WR-1	WR-2	WR-3	WR-4	WR-5	BHVO-2	
Lithology			Basaltic lava clasts					Basaltic clasts					Measured	Recommended
mbsf(cm)	13–33	34–40		41–48	48–56	56–67	67–77	34–40	41–48	48–56	56–67	67–77		
Major element oxides, wt.%														
SiO_2	48.20	47.00	47.10	47.42	47.10	47.76	45.34	34.82	42.20	45.86	45.78	45.18	49.88	49.9
TiO_2	2.78	2.72	2.70	2.74	1.89	2.92	2.63	2.03	2.46	2.39	2.51	2.38	2.71	2.73
Al_2O_3	14.21	14.23	14.22	14.69	14.52	14.38	14.05	11.20	13.09	13.11	13.49	13.18	13.7	13.5
TFe_2O_3	12.17	12.26	12.28	12.48	12.53	14.50	13.82	9.86	13.13	15.90	15.54	14.61	12.25	12.3
MnO	0.12	0.20	0.20	0.18	0.21	0.16	0.17	0.59	0.21	0.17	0.14	0.12		
MgO	4.80	4.51	4.48	4.34	4.70	4.67	4.69	3.86	4.49	5.05	5.10	5.24	7.28	7.23
CaO	11.20	11.10	11.15	11.69	11.26	8.83	10.38	19.06	11.23	5.95	6.32	8.14	11.3	11.4
Na_2O	2.90	3.00	3.02	3.09	2.01	2.73	2.84	2.37	2.91	2.95	2.94	2.87	2.25	2.22
K_2O	0.80	0.87	0.88	0.83	0.50	1.01	0.99	0.83	1.37	2.03	1.82	1.52	0.54	0.52
P_2O_5	0.67	0.67	0.65	0.78	0.62	0.45	1.19	0.47	0.71	0.17	0.22	0.69	0.26	0.27
LOI	1.20	2.72	2.68	1.77	2.73	1.88	2.61	13.37	6.65	4.48	4.40	4.80		
Total	99.05	99.28	99.36	100.01	98.07	99.29	98.71	98.46	98.45	98.06	98.26	98.73		
Mg#	54.9	52.9	52.6	51.3	50.7	48.1	49.2	54.9	49.5	45.7	46.9	49.4		
Trace element, ppm														
La	23.04	22.83	22.75	28.35	20.81	23.95	59.65	22.48	28.13	17.54	16.97	45.82	14.50	15.00
Ce	46.24	44.27	44.35	51.16	33.64	46.14	69.86	41.75	47.79	40.14	39.96	55.77	37.30	38.00
Pr	7.8	6.07	6.12	6.94	6.58	6.68	13.45	5.44	6.76	5.41	5.1	10.65		
Nd	32	26.55	26.48	30.55	29.63	29.69	59.43	23.8	29.9	23.9	22.37	46.84	24.60	25.00
Sm	8.5	6.26	6.29	7.1	7.22	7.07	13.34	5.51	6.88	5.84	5.49	10.67	5.90	6.20
Eu	2.83	2.28	2.32	2.54	2.54	2.49	4.55	1.95	2.38	2	1.94	3.59		
Gd	8.89	6.77	6.76	7.77	7.72	7.62	15.63	6.1	7.62	6.2	5.86	12.48	6.25	6.30
Tb	1.23	1.1	1.13	1.22	1.25	1.24	2.41	0.98	1.19	1.01	0.96	1.97	0.88	0.90
Dy	8.56	6.78	6.83	7.55	7.52	7.54	14.54	5.92	7.39	6.06	5.85	12.02		
Ho	1.12	1.28	1.31	1.42	1.39	1.4	2.83	1.12	1.43	1.12	1.09	2.34	1.02	1.04
Er	3.42	3.52	3.48	3.89	3.69	3.85	7.67	3.08	4	3.07	3	6.34		
Tm	0.56	0.51	0.52	0.57	0.53	0.57	1.07	0.46	0.59	0.45	0.45	0.89		
Yb	3.46	3.13	3.14	3.44	3.04	3.42	6.17	2.77	3.57	2.73	2.71	5.13	1.91	2.00
Lu	0.65	0.5	0.52	0.55	0.48	0.54	1.05	0.44	0.6	0.42	0.42	0.87	0.28	0.28
Rb	15.1	16.08	16.15	15.24	4.32	23.06	21.59	14.83	28.04	50.95	44.97	37.68	9.30	9.80
Sr	320	355	351	368	247	314	354	356	334	248	265	301	375	389
Y	43.2	36.2	36.5	44.4	31.7	39.4	103.5	36.6	47.7	28.7	28.6	82.9	25.2	26.0
Ba	489	567	549	371	128	174	592	270	153	89	94	184	123	130
Zr	180	180	183	173	120	186	170	145	166	171	176	168	168	172
Nb	35.2	33.6	34.3	33.4	25.4	37.2	32.4	27.7	32.0	31.7	34.1	31.3	17.7	18.0
Hf	4.76	4.7	4.77	4.65	4.06	5.29	4.74	3.82	4.55	4.49	4.73	4.58	4.05	4.10
Ta	2.23	2.12	2.1	2.18	1.72	2.38	2.14	1.71	2.02	1.98	2.07	1.98	1.38	1.40
Co	36.8	37.48	36.89	38.13	29.6	40.01	40.5	65.18	38.48	37.38	37.93	38.94	43.80	45.00
Cr	46.4	47.66	48.17	59.17	44.63	46.95	55.22	33.94	40.7	39.76	44.47	38.81	276	280
Cu	43.2	41.96	41.58	76.1	17.55	35.45	40.67	112.4	50.31	38.76	40.59	40.82	125	127
Ni	20.12	16.1	16.25	20.08	14.16	20.91	18.99	25.09	25.3	24.38	22.47	22.11	114	119
Sc	39.0	33.6	33.0	35.2	15.2	36.9	34.9	26.2	30.9	30.5	31.3	30.9	31.4	32.0
V	380	347	357	348	239	358	343	222	272	266	270	267	308	317
Zn	146	131	131	140	84	120	169	97	110	104	103	133	99	103
Pb	10.2	13.42	12.98	9.21	1.03	1.63	8.41	3.8	4.45	1.47	1.58	8.46		
Th	2.12	2.26	2.3	2.27	0.92	2.53	2.24	1.79	2.16	2.11	2.22	2.1	1.12	1.20
U	0.78	0.64	0.67	0.74	0.28	0.48	0.64	0.39	0.58	0.51	0.47	0.53		

is ~21 km at the base and decreases to ~3 km at the summit. The water depths at the base and top of the seamount are 4000 m and 1978 m, respectively (Fig. 1C).

The core samples analyzed in this study were taken through shallow-drilling on the slope (water depth is about 2300 m) of Daimao Seamount. This drilling was carried out by the Guangzhou Marine Geological Survey, Ministry of Land and Resources of the People's Republic of China. The total length of the core is 770 mm and it can be divided into three segments. From top to bottom (Fig. 2), these are: (I) Fe–Mn oxide crust (0–130 mm), (II) carbonate deposits embedded with some basaltic lava rubble (130–340 mm), and (III) basaltic lava breccia-bearing volcaniclastic rocks (340–770 mm). Our petrologic investigation mostly focuses on the clasts of basaltic lava breccias in segment III; these clasts are henceforth called 'basaltic breccias'. Segment III was further divided into five sub-segments in order to elucidate the possible variations in magma composition during eruptions. Five least-altered basaltic breccias from segment III were sampled, one each from the five sub-segments along with a basaltic lava clast from Segment II (sample BBL) (Fig. 2). Five whole-rock samples of the volcaniclastic host located close to the basaltic breccias in segment III were also sampled for comparison. Detailed sample locations are shown in Fig. 2 and Table 1. Note that most of the basaltic breccias in segment III and the basaltic lava clast in segment II are angular, suggesting these were products of *in situ* or nearby volcanism.

3. Analytical methods

3.1. Sample preparation

Whole volcaniclastic rock samples (depths from 340 to 770 mm of the drill core) from the five sub-segments in segment III (Fig. 2) and from segment II were first crushed into centimeter-sized chips with a hydraulic press and, then, the chips were further subdivided into two identical parts. From one part, fragments of relatively fresh basaltic

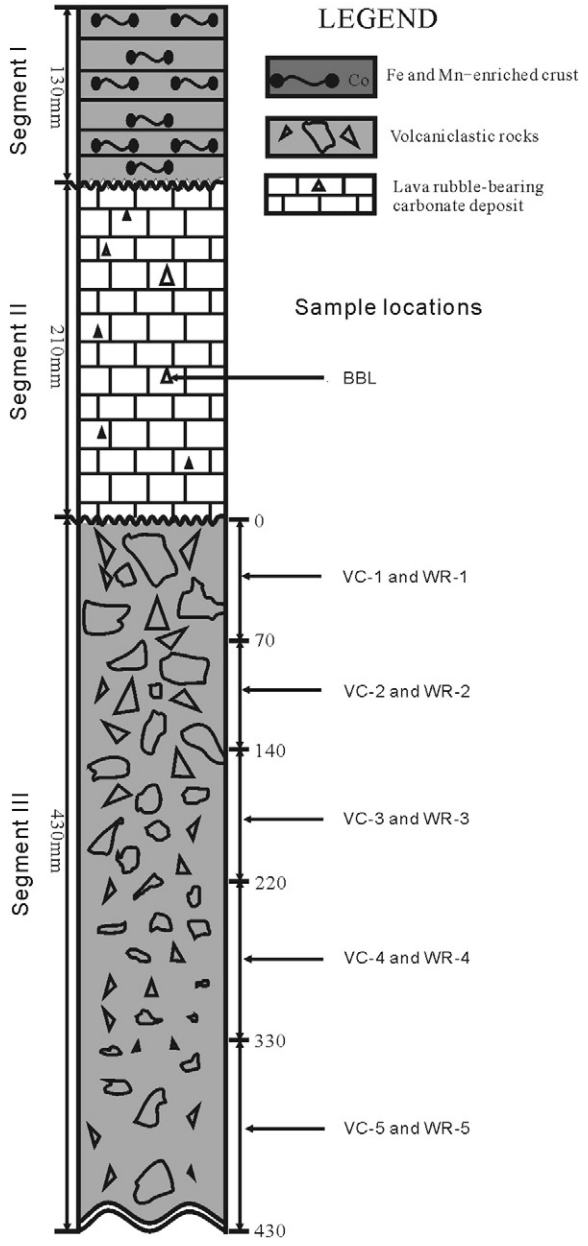

Fig. 2. Lithologies and sample locations of the drill core from Daimao Seamount. Segment I: Fe–Mn oxide crust (0–1300 mm); Segment II: carbonate deposits embedded with basaltic breccias (130–340 mm); and Segment III: volcaniclastic rock containing ks basaltic breccias (340–770 mm). In Segment III, from 0 to 330 mm, basaltic breccias decrease in amount and become smaller in size; from 330 to 430 mm, basaltic breccias are fewer in abundance relative to those in the 0–330 mm part, but are generally bigger in size. Some basaltic breccias appear fresh, some are partially altered, and some of the smaller ones are totally altered. The figure also shows the sampling locations within Segment III (i.e., VC-1 and WR-1 are from 0–70 mm, VC-2 and WR-2 are from 0–70 mm, VC-3 and WR-3 are from 0–70 mm, VC-4 and WR-4 are from 0–70 mm, and VC-5 and WR-5 are from 0–70 mm).

breccias were picked under a binocular microscope. Then both bulk volcaniclastic rocks and basaltic breccias were powdered in an alumina ceramic mill. Details of the sample preparation work are the same as those described by Janney and Castillo (1996). The powdered samples were analyzed for major element, trace element and Sr–Nd–Pb isotopic compositions. In order to obtain the primary composition of the basaltic breccias and the possible effects of secondary seawater alteration on the samples, we analyzed the age, major- plus trace-element and Sr–Nd–Pb isotopic compositions of both the basaltic breccias and whole rock samples.

3.2. K–Ar dating methods

Based on detailed petrographic observations, we selected one basaltic breccia sample (sample VC-5, from the lowest part of the core) to be dated. The analytical work was carried out in the State Key Laboratory of Earthquake Dynamic (SKLED), Institute of Geology, China Earthquake Administration. The detailed dating method is the same as described by Yan et al. (2008b). Parameters for age calculation are the follows, $^{40}Ar/^{36}Ar = 295.5$; $\lambda = 5.543 \times 10^{-10}\ a^{-1}$; $\lambda_\beta = 4.962 \times 10^{-10}/a$; $\lambda_e = 0.581 \times 10^{-10}/a$; $^{40}K/K = 1.167 \times 10^{-4}$ mol/mol.

3.3. Major- and trace element analysis

The SiO_2 contents of the samples were analyzed by X-ray fluorescence (XRF) PW-1500 at No. 4 Exploration Institute of Geology and Mineral Resources of Shandong province (China) whereas the other major element oxides and certain trace elements (e.g., Ba, Cu, Sr, V, Zn and Cr) were determined by inductively coupled plasma-optical emission spectrometry (ICP-OES) (Agilent 7200, Thermo-Scientific, Waltham, MA, USA) at Key Laboratory of Marine Sedimentary and Environmental Geology, State Oceanic Administration (KLMSEG-SOA) (China). Samples were prepared by digesting 50 mg of powder with a HF–HNO_3 (2:1) mixture following the method described by Janney and Castillo (1996). Precisions are ±0.2% to 2% for major elements in concentrations >1 wt.% (SiO_2, Al_2O_3, and CaO) and about ±2% to 5% for minor elements in concentrations <1.0 wt.% (MnO, K_2O, TiO_2, and P_2O_5). Loss in ignition (LOI) was also measured. The precision of this method for trace elements is >10%. Concentrations of trace elements including high field strength elements (HFSE) (except for Zr), rare earth elements (REE) and other trace elements (e.g., Li, Be, Cr, Co, Ni, Ga, Rb, Mo, Cd, In, Cs, W, Tl, Bi, Sc, U, Th and Pb) were measured using a X SeriesII inductively coupled plasma-mass spectrometer (ICP-MS) (Thermo-Scientific, Waltham, MA, USA), also at KLMSEG-SOA. The procedures for sample preparation and instrument analysis are similar to those for ICP-OES. The precision of this method is within 10%. The measured and recommended values for BHVO-2 (international standard sample) for the present study are also presented in Table 1.

3.4. Sr–Nd–Pb isotopic analysis

Sr and Nd isotopic analyses were carried out for five whole rock samples and five basaltic breccias from Segment III, and one sample from Segment II. Pb isotopic analysis was carried out for three whole rock samples and three basaltic breccias from Segment III, and one sample from Segment II. Prior to dissolution, rock powders to be analyzed for Sr isotopic ratios were first put through a harsh, multi-step, HCl-leaching procedure (e.g., Castillo et al., 1991) to mitigate the effects of seawater alteration on $^{87}Sr/^{86}Sr$ ratios. The Sr and Nd separation procedure used is similar to that described by Janney and Castillo (1996). For Pb isotopic analysis, chips of the fresh basaltic breccias were leached with ultrapure 6 N nitric acid for 6 h in an ultrasonic bath to remove possible Pb contamination. Then the samples were rinsed with quartz-distilled water, dried and crushed in a tungsten carbide shatterbox. Lead was separated using a standard anion exchange method in an HBr medium (Lugmair and Galer, 1992). Details of the Pb separation procedure are presented in Janney and Castillo (1996). Sr, Nd, and Pb isotopic ratios were measured on a high-resolution, multi-collector inductively coupled plasma-mass spectrometer (Nu Instruments Ltd., Wrexham, North Wales, UK) at KLMSEG-SOA. $^{143}Nd/^{144}Nd$ ratios were normalized to $^{146}Nd/^{144}Nd = 0.7219$ and $^{87}Sr/^{86}Sr$ ratios to $^{86}Sr/^{88}Sr = 0.1194$. During the period of analysis, NBS987 standard yielded an average value of $^{87}Sr/^{86}Sr = 0.710265 \pm 12(2\sigma)$ and Jndi-1 standard gave an average value of $^{143}Nd/^{144}Nd = 0.512119 \pm 8(2\sigma)$. Procedural blanks were <200 pg for Sr and <50 pg for Nd. Pb standard NBS 981 was used to correct the measured isotopic ratios of samples for isotopic fractionation, and the average correction is 0.1% per atomic mass unit. During the

analysis, NBS981 standard yielded an average value of $^{206}Pb/^{204}Pb$ = 16.9379, $^{207}Pb/^{204}Pb$ = 15.4936, and $^{208}Pb/^{204}Pb$ = 36.7244. Initial Pb isotopic ratios were calculated from measured ratios in unleached samples using the U, Th, and Pb concentrations of the samples.

4. Results

The newly obtained K–Ar age for sample VC-5 from Daimao Seamount is 16.6 ± 0.8 Ma (±1σ) and this represents the apparent crystallization age of this sample. Related values for this measurement work are as follows: K = 0.60%, $^{40}Ar_{rad}$(g mol/g) = 1.73×10^{11}, and $^{40}Ar_{rad}$ = 50.92%.

Major and trace element compositions are reported in Table 1. Loss in ignition values of the five basaltic breccias range from 1.20 to 2.73 wt.%, much less than those of the five volcaniclastic rocks (4.40–13.37 wt.%) (Table 1). This is consistent with petrographic characteristics, i.e., a large amount of several types of hydrous/alteration minerals are present in the volcaniclastic rocks whereas almost none are present in the breccias. Basaltic breccias, as well as most of the volcaniclastic rocks, belong to the alkaline lava series, similar to the alkali basalts from other seamounts in the SCS (Fig. 3a and b, Yan et al., 2008a) but are different from the tholeiitic basalts previously dredged from this seamount (Tu et al., 1992).

Relative to the alkali basalts from other SCS seamounts (Yan et al., 2008a), the concentrations of large ion lithophile elements (LILE — e.g., Rb, Sr, Th, U), Nb and Ta in the basaltic breccias from Daimao Seamount are distinctly lower, whereas those of Zr and Hf are nearly identical (Fig. 4a). Some of the differences, particularly the LILE concentrations, are most probably due to seawater alteration. Compared to typical ocean island basalts (OIB), however, their LILE concentrations are also lower and their Nb and Ta concentrations have smaller positive anomalies. These, combined with their lower light/heavy REE ratios [$(La/Yb)_N$ = 4.8–6.9] relative to OIB [$(La/Yb)_N$ = 12.3, Niu and O'Hara, 2003] (Fig. 4b), indicate that the basaltic breccias from Daimao Seamount were produced by a higher degree of partial melting than the alkali basalts from other SCS seamounts, assuming that they all came from the same source (Yan et al., 2008a; see additional discussion below). In general, however, the trace element concentration patterns from Daimao Seamount are similar to those of OIB, although their bulk concentrations lie between those of enriched-MORB and other SCS seamounts (Fig. 4). With the exception of their Rb, Ba and K contents, the five bulk volcaniclastic rocks generally have similar trace element concentration patterns to the basaltic breccias (Table 1, Figs. 4 and 5).

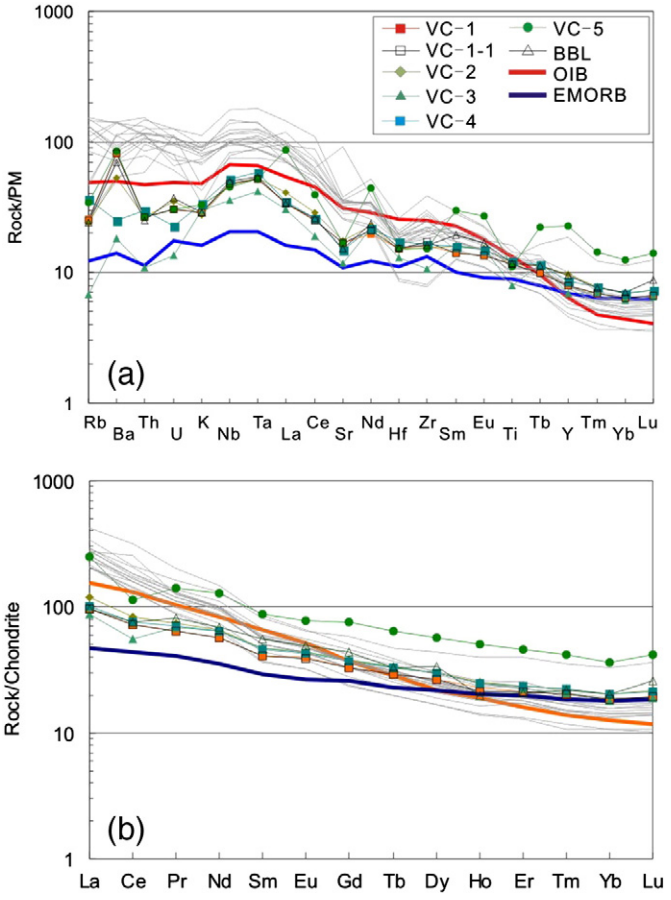

Fig. 4. Primitive mantle-normalized incompatible trace element concentrations (a) and chondrite-normalized REE concentration patterns (b) for basaltic breccias separated from the volcaniclastic rock samples from the drill core in Daimao Seamount. Trace element abundances of the primitive mantle (PM) and chondrites are from Sun and McDonough (1989). OIB and enriched-MORB average values are from Niu and O'Hara (2003). Gray lines are for basalts from other seamounts in the SCS (Yan et al., 2008a).

The Sr, Nd and Pb isotopic analyses are listed in Table 2. The six basaltic breccias have relatively homogeneous isotopic compositions (Fig. 6). Compared to the basaltic breccias, the five volcaniclastic rocks have higher $^{87}Sr/^{86}Sr$ ratios, but have homogeneous $^{143}Nd/^{144}Nd$ ratios, identical to the $^{143}Nd/^{144}Nd$ ratios of the basaltic breccias (Table 2,

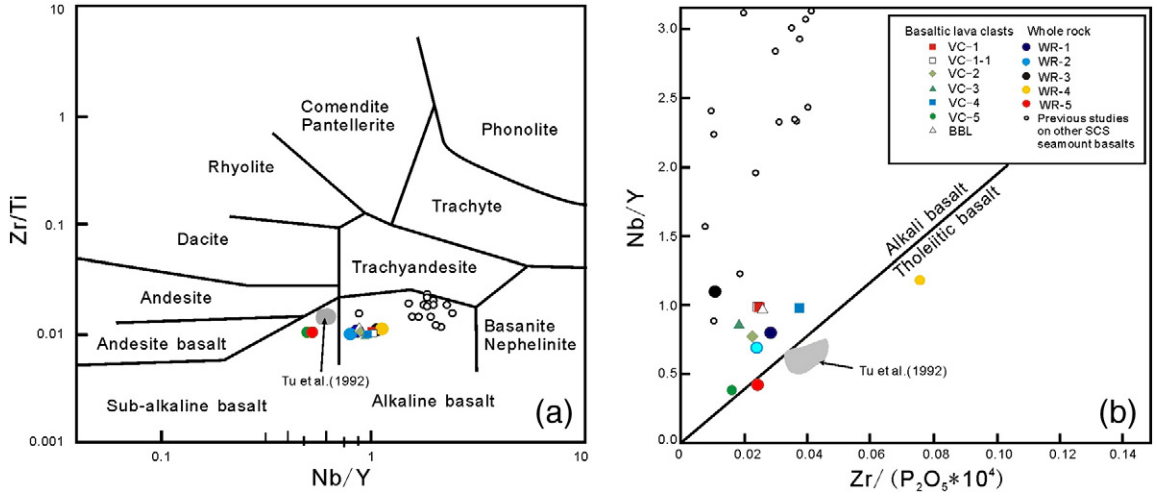

Fig. 3. (a) Zr/Ti vs. Nb/Y (Winchester and Floyd, 1977) and (b) Nb/Y vs. Zr/(P_2O_5*10^4) (Floyd and Winchester, 1975) discriminant diagrams for samples from the drill core in Daimao Seamount. Data from previous studies on other seamount SCS basalts are from Yan et al. (2008a). Data for tholeiites from this seamount (gray field) are from Tu et al. (1992).

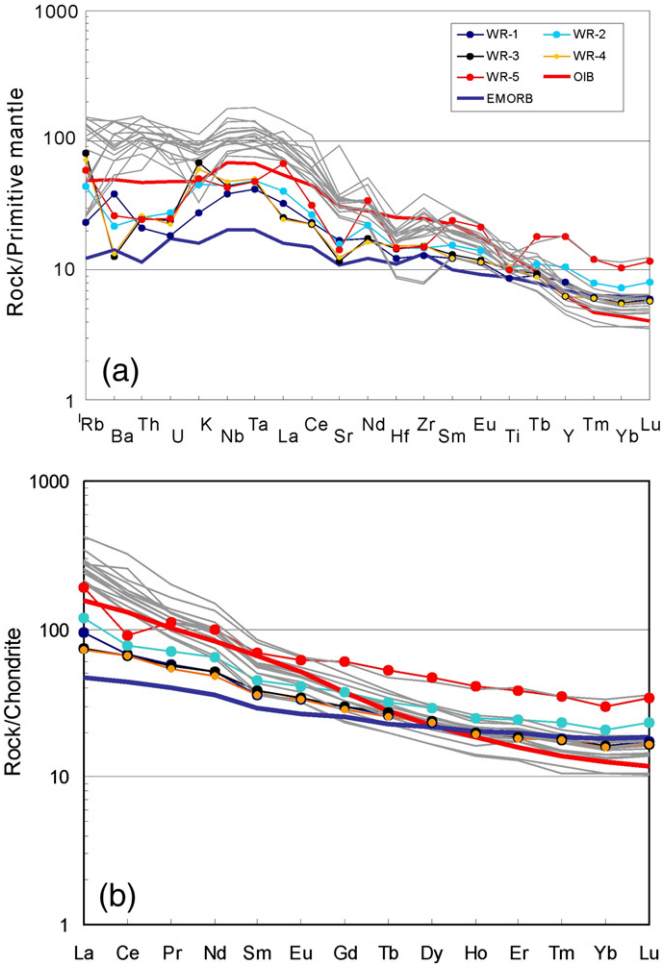

Fig. 5. Primitive mantle-normalized incompatible trace element concentrations (a) and REE distribution patterns (b) for whole rock samples from Daimao Seamount. Data for primitive mantle and chondrites are from Sun and McDonough (1989). Data for enriched MORB mantle (EMORB) are from Niu and O'Hara (2003).

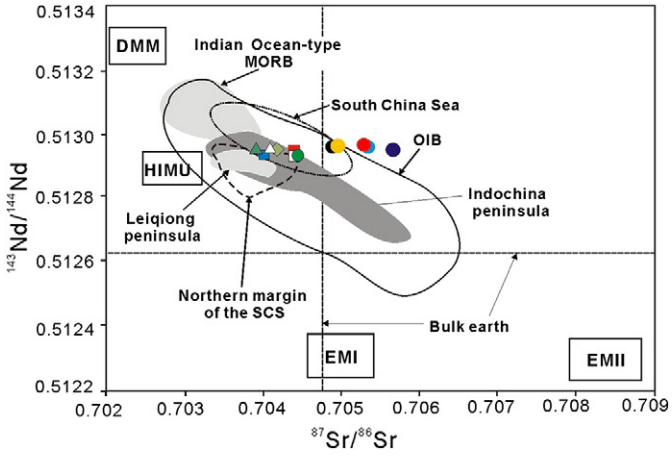

Fig. 6. $^{87}Sr/^{86}Sr$ versus $^{143}Nd/^{144}Nd$ plots for volcanic rocks from Daimao Seamount. The approximate fields for DMM, HIMU, EM1, and EM2 are from Zindler and Hart (1986), for OIB is from Castillo (1988) and for Indian Ocean-type MORB is from Mahoney et al. (1989). Data for the Leiqiong peninsula are from Tu et al. (1991) and Zou and Fan (2010). Data for northern margin of the SCS including Zhujiangkou basin, Niutoushan and Penghu basalts are from Zou et al. (1995), Zou et al. (2000, 2004) and X.-C. Wang et al. (2012). South China Sea refers to previous study on the other seamount of the SCS (Yan et al., 2008a). Symbols are the same as in Fig. 3.

Fig. 6). The Sr and Nd isotope systematics of the volcaniclastic rocks undoubtedly reflect the influence of low-temperature seawater alteration on Sr, but not Nd, isotopes. Significantly, it appears that the acid-leaching procedure did not completely remove the effects of seawater alteration on the $^{87}Sr/^{86}Sr$ ratios of the basaltic breccias.

The Pb isotopic compositions of the basaltic breccias are less radiogenic in $^{206}Pb/^{204}Pb$ and $^{208}Pb/^{204}Pb$ (Table 2, Fig. 7) than the volcaniclastic rocks and this probably also reflects the influence of low-temperature seawater alteration on the Pb isotopes.

5. Discussion

Since the majority of Hainan basalts and other SCS seamount basalts are younger than 8 Ma (e.g., Flower et al., 1992; Hoang and Flower, 1998; Yan et al., 2008b; Zhou and Mukasa, 1997; Zou and Fan, 2010) and the alkaline Daimao Seamount basaltic breccias have an OIB-like composition, the 16.6 Ma Daimao Seamount may represent an "early" manifestation of the Hainan plume volcanism. We note that some contemporaneous and/or younger basalts in and around the southern Taiwan Strait (Niutoushan basalts — 15.7 ± 0.6 Ma and Penghu basalts — 8.2–11.8 Ma; Ho et al., 2003; X.-C. Wang et al., 2012; Zou et al., 2000, 2004) are also compositionally similar (Figs. 6 and 7) to seamount basalts from the SCS region (Yan et al., 2014). The compositional similarity indicates that these basaltic magmas may also belong to the intraplate volcanism that formed around SCS basin after the cessation of spreading. Therefore, intraplate volcanism in the South China Sea region may be more widespread than previously believed (see also, Hoang et al., 1996; Shi and Yan, 2011; Xu et al., 2012; Yan et al., 2014).

5.1. Petrogenesis of volcanic rocks from Daimao Seamount

The LOI values of the bulk volcaniclastic rocks correlate with their K_2O, CaO, MgO, Rb, and $^{87}Sr/^{86}Sr$ values (Tables 1 and 2; not shown), suggesting that seafloor alteration may have affected the major and trace element contents as well as the Sr isotopic composition of these

Table 2
Nd–Sr–Pb isotopic compositions in volcanic rocks from the Daimao Seamount, the South China Sea.

Sample no.	$^{87}Sr/^{86}Sr$	Error (2σ)	$^{143}Nd/^{144}Nd$	Error (2σ)	$^{206}Pb/^{204}Pb$	Error (2σ)	$^{207}Pb/^{204}Pb$	Error (2σ)	$^{208}Pb/^{204}Pb$	Error (2σ)
BBL	0.704105	0.000010	0.512964	0.000060	18.867	0.00024	15.603	0.00025	38.861	0.00017
VC-1	0.704477	0.000012	0.512961	0.000005	18.860	0.00027	15.586	0.00029	38.804	0.00026
VC-1-1	0.704475	0.000012	0.512958	0.000060	18.861	0.00025	15.586	0.00027	38.804	0.00022
VC-2	0.704238	0.000014	0.512967	0.000004	18.717	0.00019	15.623	0.00023	38.851	0.00014
VC-3	0.703909	0.000014	0.512963	0.000004						
VC-4	0.704036	0.000022	0.512957	0.000004						
VC-5	0.704642	0.000011	0.512958	0.000003	18.668	0.00009	15.620	0.00009	38.819	0.00025
WR-1	0.705710	0.000014	0.512959	0.000004	18.943	0.00014	15.558	0.00010	38.892	0.00029
WR-2	0.705336	0.000014	0.512961	0.000004	18.970	0.00009	15.571	0.00030	38.942	0.00016
WR-3	0.704896	0.000009	0.512960	0.000004						
WR-4	0.704912	0.000015	0.512962	0.000004						
WR-5	0.705306	0.000011	0.512963	0.000005	18.938	0.00009	15.570	0.00029	38.909	0.00016

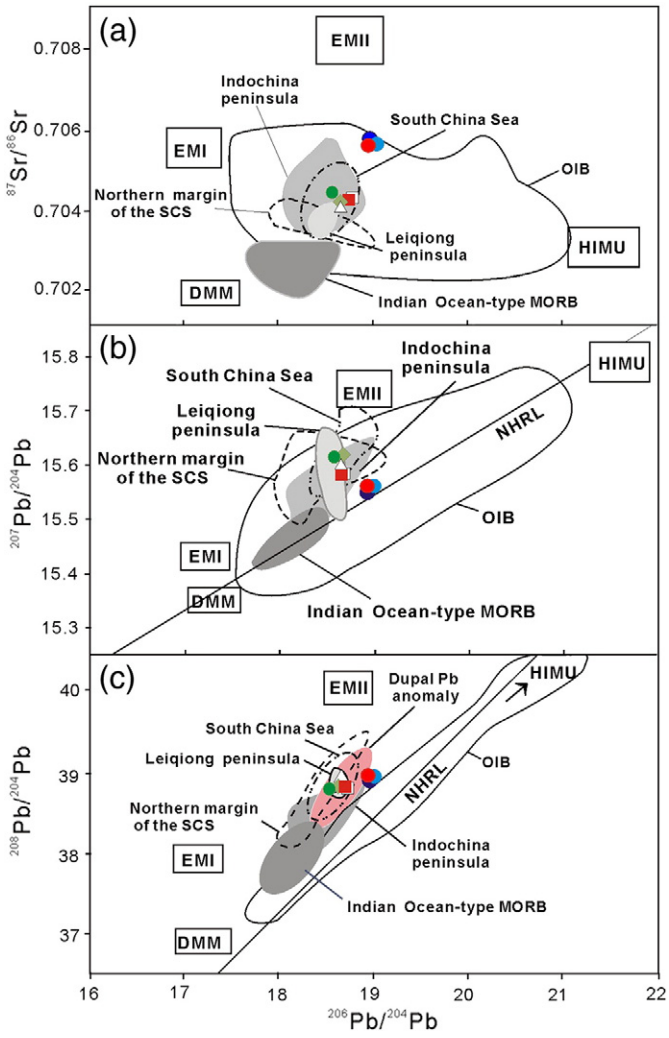

Fig. 7. (A) $^{87}Sr/^{86}Sr$ versus $^{206}Pb/^{204}Pb$, (B) $^{208}Pb/^{204}Pb$ versus $^{206}Pb/^{204}Pb$, and (C) $^{207}Pb/^{204}Pb$ versus $^{206}Pb/^{204}Pb$ plots for samples from Daimao Seamount. Symbols and data sources as in Fig. 6. NHRL is the North Hemisphere reference line (Hart, 1984). The field for the Dupal anomaly is from Hamelin and Allègre (1985). Other data sources are the same as those in Fig. 6; symbols are the same as in Fig. 3.

samples. However, similar data for the basaltic breccias separated from the volcaniclastic rocks do not display such relationships. As the effects of seawater alteration cannot be completely ruled out in the basaltic breccias, we rely on the more alteration-resistant HFSE and REE as well as Nd and Pb isotopic compositions of the basaltic breccias to interpret their petrogenesis and its implications for the tectonic setting. Data for the bulk volcaniclastic rocks are used simply for comparison purposes.

In general, the volcanic rocks from Daimao Seamount and other seamounts in the SCS (Yan et al., 2008a) were formed in an intraplate tectonic setting, similar to those in the nearby Leiqiong peninsula (reviewed by Yan et al., 2014). Thus, post-spreading intraplate volcanism has extensively affected the South China Sea region (Hoang et al., 1996; Shi and Yan, 2011; Xu et al., 2012; Yan et al., 2014).

Trace element ratios typically used as petrogenetic tracers (e.g., Nb/Ta, Zr/Hf, Nb/U, and Ce/Pb) for the basaltic breccias from Daimao Seamount (Table 1) lie within the range of OIB (Hofmann, 1988; Niu and O'Hara, 2003), similar to other SCS seamounts (Yan et al., 2008a, 2008b). These ratios (Table 1) as well as their Sr–Pb isotope compositions (Table 2) are quite variable, implying that their source is slightly heterogeneous.

As shown in Fig. 8 (see also, Figs. 6 and 7), the source of the basaltic breccias can be explained by binary mixing between a proposed depleted mantle source of MORB (DMM) and enriched mantle II (EMII; Zindler and Hart, 1986). The latter has been proposed as the main component of the Hainan mantle plume (X.-C. Wang et al., 2012; Yan et al., 2008a; Zou and Fan, 2010). Moreover, Daimao Seamount samples also possess the so-called Dupal isotopic anomaly (i.e., high $^{87}Sr/^{86}Sr$ — generally >0.7030, and high $^{207}Pb/^{204}Pb$ and $^{208}Pb/^{204}Pb$ for a given $^{206}Pb/^{204}Pb$; Castillo, 1988; Hart, 1984), similar to the other SCS seamounts (Tu et al., 1992; Yan et al., 2008a). The latter implies an endogenous Dupal mantle component beneath the SCS (Tu et al., 1992; Yan et al., 2008a), instead of the anomaly being introduced beneath the SCS from specific regions in the mantle (e.g., Castillo, 1996; Straub et al., 2009).

The trace element characteristics (Fig. 4) also indicate that the degree of partial melting of the mantle beneath Daimao is higher than the other SCS seamounts (Fig. 9, cf. Yan et al., 2008a). Significantly, the incompatible trace element ratios of Daimao Seamount basaltic breccias are similar to those of OIB (Table 1), suggesting that the parental magmas of Daimao (oceanic) basalts did not experience crustal contamination (Yan et al., 2008a). Notably, even the parental magmas for the Hainan Quaternary basalts that erupted through thick continental crust in the Leiqiong Peninsula did not undergo crustal contamination (X.-C. Wang et al., 2012; Zou and Fan, 2010). However, their relatively low MgO contents (and Mg# = 48–55 for basaltic breccias, Table 1) and compatible element contents (e.g., Cr, Co, Ni, Sc) suggest that the parental magmas of the Daimao basaltic breccias most likely experienced extensive fractional crystallization of olivine and/or clinopyroxene during their ascent and/or storage in high level magma chambers.

5.2. Relationship between seafloor spreading and intraplate volcanism in marginal basins

Volcanic seamounts near fossil spreading centers are common in the Oligocene to Miocene SCS, Shikoku and Sea of Japan basins in the western Pacific marginal basins. However, the relationship between their time of formation and seafloor spreading is poorly understood and, thus, their origin and geodynamic importance are still unclear (e.g., Ishizuka et al., 2009; Kaneoka et al., 1990; Klein et al., 1978; Pouclet et al., 1995; Tu et al., 1992; Yan et al., 2008a, b).

In the Shikoku and Sea of Japan basins, seamounts were formed immediately after the cessation of seafloor spreading (e.g., Ishizuka et al., 2009; Kaneoka et al., 1990; Klein et al., 1978; Pouclet et al., 1995). However, the SCS underwent three episodes of seafloor spreading (Briais et al., 1993) and the intraplate seamounts here were formed 6–12 my after the cessation of spreading. For example, Jianfeng Seamount (18.6 Ma, Wang et al., 1984) in the northwest sub-basin was formed 10 my after the cessation (corresponding to magnetic anomaly 10) of spreading in the 18°N fossil spreading center, seamounts in the Scarborough chain were formed 6–12 my after the cessation (16 Ma) of the 15.5°N fossil spreading center, and Daimao Seamount (16.6 Ma) was formed 10 my after the cessation of spreading (corresponding to magnetic anomaly 8) in the 17°N fossil spreading center.

The mantle sources of Shikoku and Sea of Japan marginal basin basalts (e.g., Ishizuka et al., 2009; Kaneoka et al., 1990; Klein et al., 1978; Pouclet et al., 1995) were generated through mixing between DMM and the proposed enriched mantle type I (EMI) (Pouclet et al., 1995). Moreover, detailed studies indicate that the EMI component does not originate from a mantle plume, but instead occurs as enriched heterogeneities or blobs dispersed in the upwelling asthenosphere. This scenario is similar to the distribution of enriched mantle source of near-ridge seamount basalts in the eastern Pacific (Castillo et al., 2010). In contrast, the intraplate magmatism that formed SCS seamounts also occurred in the surrounding areas (Indochina block, Leiqiong peninsula in the northern margin of the SCS) (e.g., Flower et al., 1992; Hoang and Flower, 1998; Zhou and Mukasa, 1997; Zou and Fan, 2010) and has continued to the Quaternary (X.-C. Wang et al., 2012; Zou and Fan, 2010).

As discussed above (see also, Fig. 8), the mantle sources of these intraplate seamounts were generated through mixing between DMM and EMII (reviewed by Yan et al., 2014), and the EMII may have originated

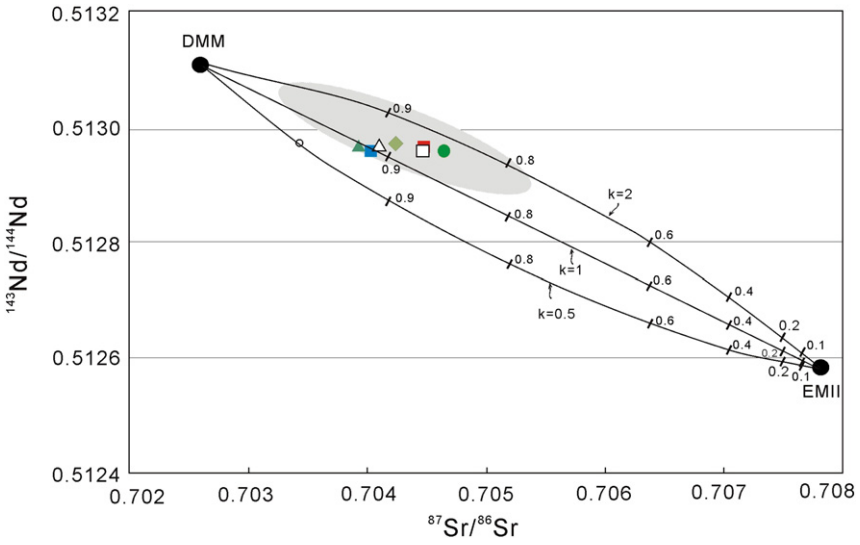

Fig. 8. A simple two end-member mixing model to explain the origin of volcanic rocks from Daimao Seamount. End-member compositions are (1) DMM (depleted MORB mantle): Sr (ppm) = 7.66, Nd (ppm) = 0.58, $^{87}Sr/^{86}Sr = 0.7026$, $^{143}Nd/^{144}Nd = 0.51311$ (Workman and Hart, 2005) and (2) EMII (enriched mantle II): $^{87}Sr/^{86}Sr = 0.7078$, $^{143}Nd/^{144}Nd = 0.51258$ (Hart et al., 1992). Tick marks with numbers represent % contributions from the DMM to the mixture. In general, Daimao Seamount breccias can be produced by adding about 92–87% DMM melt to EMII melt. Data for the other seamounts in the SCS (Yan et al., 2008a) are also plotted (gray field). Symbols are the same as in Fig. 3.

from the Hainan mantle plume whose existence has been supported by recent geophysical data (Lebedev and Nolet, 2003; Lei et al., 2009; Montelli et al., 2006; Zhao, 2007). When such a plume ascends to the bottom of the lithosphere, it may migrate along sloping rheologic boundary layers (Kincaid et al, 1995) to lithospheric faults under extensional settings (e.g., reactivated paleo-sutures, spreading centers),

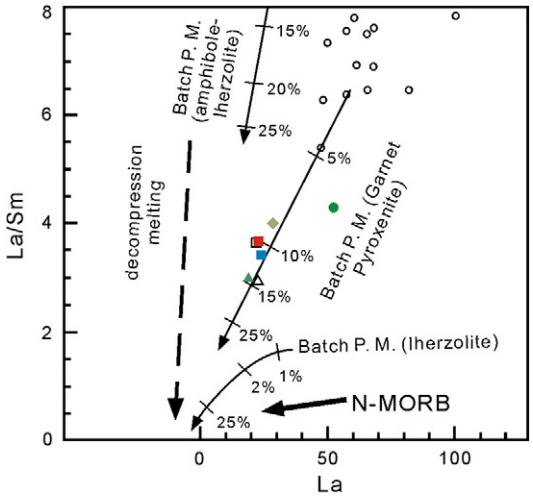

Fig. 9. La versus La/Sm diagram that schematically illustrates the effect of variations in the degree of decompression partial melting of different mantle sources on the composition of mantle melts. At one extreme, vigorous upwelling and melting produce low La and La/Sm values (e.g., normal-MORB) from a lherzolite mantle. In the other extreme, weak upwelling and melting produce relatively higher La and La/Sm values (e.g., Davidson Seamount basalts, Castillo et al., 2010) from an amphibole-rich and/or carbonatite-metasomatized lherzolite. Curves with tick marks represent equilibrium batch partial melting of an olivine:orthopyroxene:clinopyroxene:spinel (54:27:13:6 mixture) lherzolite, an amphibole-rich lherzolite (55:20:05:15:05 amphibole:olivine:orthopyroxene:clinopyroxene:-garnet) and a garnet pyroxenite (50:45:5 garnet:orthopyroxene:clinopyroxene); percent at each tick mark represents degree of melting. For melting calculations the following parameters were used: bulk D for La was 0.0015 and for Sm was 0.0406 in the lherzolite; bulk D for La was 0.089 and for Sm was 0.579 in the amphibole-lherzolite; bulk D for La was 0.0246 and for Sm was 0.236 in the garnet pyroxenite. As shown, the parental basalts for Daimao Seamount breccias were produced by 9 to 15% partial melting of garnet pyroxenite. Fractional crystallization increases both La and Sm approximately equally (represented by horizontal line labeled F.C.). Data for the other seamounts in the SCS (Yan et al., 2008a) are also plotted (small circles). Symbols are the same as in Fig. 3.

eroding the lithosphere on its way upward (i.e., lithosphere/plume interaction) (e.g., Yan et al., 2014). Alternatively, Hainan plume materials may have been accumulating under the region for a significant period of time and the ponded plume materials are being sampled by the spreading centers that generally "young" to the south.

Finally, the opening and post-spreading processes in both the Shikoku and Sea of Japan basins are closely related to the subduction of Pacific Plate (e.g., Ishizuka et al., 2009; Pouclet et al., 1995). However, there is no direct evidence that the formation of the SCS is related to any nearby subduction zone (e.g., Karig, 1971; Tapponnier, 1986) although this possibility cannot be completely ruled out. Therefore, the magmatism associated with the formation and evolution of the SCS is different from that in other western Pacific marginal basins.

5.3. A tectonic evolution scenario for Daimao Seamount

The occurrence of volcaniclastic rocks and shallow-water carbonate facies near the summit of Daimao Seamount (Fig. 2) suggests that the seamount was formed by subaqueous explosive volcanism at a depth above the pressure compensation level for explosive volcanism (e.g., Fisher, 1984; McBirney and Murase, 1970). Then, the seamount subsided and experienced a period of relative quiescence that allowed carbonate sedimentation to occur and, possibly, small volume effusive basaltic eruptions near sea level, as evidenced by the basaltic breccia fragments in the shallow-water carbonate deposit (Fig. 2). Significantly, subaqueous explosive eruptions may have been widely distributed in the SCS, as evidenced in other seamounts, and where alkali basalt-type magmatism may have predominated (Yan and Shi, 2009).

The water depth at the summit of Daimao Seamount at present is 1978 m, deeper than similar-sized Zhangzhong (1290 m) and Zhenbei (1480 m) seamounts located near the 15.5°N fossil spreading center that were formed by subaqueous explosive eruptions (Yan and Shi, 2009). Based on isostasy, the current depths of these seamounts are consistent with their ages — i.e., the 16.6 Ma Daimao Seamount is older than the latter two, ~7.5 Ma seamounts (Yan et al., 2008b). From the subaqueous volcanic eruption of Daimao Seamount at 16.6 Ma to its present 1978 m depth, its estimated mean subsidence rate is 0.12 mm/y (1978 m/16.6 Ma). This value is less than the estimated subsidence rates for Zhangzhong (0.26 mm/y) and Zhenbei (0.30 mm/y) seamounts (Yan and Shi, 2009). However, provided that the geodynamic setting of Daimao Seamount is similar to those of the Zhangzhong and

Zhenbei seamounts, the slower mean subsidence rate of the former relative to the latter two is consistent with the proposal by Pritchard and Simons (2002) that the subsidence rate of submarine volcanic edifices decreases with time.

6. Conclusions

The volcanic rocks from Daimao Seamount (near the 17°N fossil spreading center) are products of intraplate volcanism at 16.6 Ma. Geochemical compositions show that mantle sources of these volcanics are generated through mixing between DMM and EMII (possibly the Hainan mantle plume), and that there is an endogenous Dupal mantle component beneath the SCS.

Volcanic seamounts near fossil spreading centers are common in Oligocene to Miocene marginal basins (e.g., South China Sea (SCS), Shikoku and Sea of Japan basins) in the western Pacific, but the relationship between their formation time and seafloor spreading may be different in different basins, and their origins are also different. Volcanic seamounts in the SCS generally were formed 6–12 my after the cessation of Cenozoic spreading, and yet those in Shikoku and Sea of Japan basins were formed immediately after the cessation of the spreading. In addition, volcanics from seamounts in the Shikoku and Sea of Japan basins contain a subduction component whereas those from the SCS do not.

Based on our new and existing data, we propose a model for the origin and evolution of Daimao Seamount in the SCS: at about 16.6 Ma, the basaltic foundation of Daimao Seamount was formed by subaqueous explosive volcanism from materials from the Hainan mantle plume. The seamount initially subsided fairly rapidly (>0.12 mm/y), allowing coral-bearing carbonate deposition on its summit area. Subsidence continued with time to the present depth but at a decreasing rate (<0.12 mm/y). Combined data also show that SCS seamounts generally show a younging trend consistent with the ages of underlying oceanic crusts, becoming younger from the northwest sub-basin to the Scarborough seamount chain, which suggests that the southward ridge jumps and cooling and thickening of the basin lithosphere may have been due to the influence of the relatively stationary Hainan mantle plume on the northward-migrating spreading centers.

Acknowledgments

We thank Haibo Zou, Greg Shellnutt and an anonymous reviewer for reviewing this manuscript, and Andrew Kerr for editorial handling and helpful comments. This study was supported by National Natural Science Foundation of China (grant no. 41322036, 41230960, 41276003), Youth Foundation for Marine Sciences of State Oceanic Administration of the PRC (grant no. 2011303), China Ocean Mineral Resources R&D Association (COMRA) (grant no. DY125-12-R-05), China Postdoctoral Science Foundation (grant no. 201104616), and Taishan Scholarship from Shandong Province.

Appendix A. Supplementary data

Supplementary data to this article can be found online at http://dx.doi.org/10.1016/j.lithos.2014.12.023.

References

Briais, A., Patriat, P., Tapponier, P., 1993. Updated interpretation of magnetic anomalies and seafloor spreading stages in the South China Sea: implications for the Tertiary Tectonics of Southeast Asia. Journal of Geophysical Research 98 (B4), 6299–6328.

Cande, S.C., Kent, D.V., 1995. Revised calibration of the geomagnetic polarity timescale for the Late Cretaceous and Cenozoic. Journal of Geophysical Research 98, 6299–6328.

Castillo, P., 1988. The Dupal anomaly as a trace of the upwelling lower mantle. Nature 336, 667–670.

Castillo, P., 1996. Origin and geodynamic implication of the Dupal isotopic anomaly in volcanic rocks from the Philippine island arcs. Geology 24, 271–274.

Castillo, P., Carlson, R., Batiza, R., 1991. Origin of Nauru Basin igneous complex: Sr, Nd and Pb isotope and REE constraints. Earth and Planetary Science Letters 103, 200–213.

Castillo, P., Clague, D., Davis, A., Lonsdale, P.F., 2010. Petrogenesis of Davidson Seamount lavas and its implications for fossil spreading center and intraplate magmatism in the eastern Pacific. Geochemistry, Geophysics, Geosystems 11, Q02005. http://dx.doi.org/10.1029/2009GC002992.

Chung, S.-L., Cheng, H., Jahn, B.M., O Reilly, S.Y., Zhu, B.Q., 1997. Major and trace element, and Sr–Nd isotope constraints on the origin of Paleogene volcanism in South China prior to the South China Sea opening. Lithos 40, 203–220.

Fisher, R.V., 1984. Submarine Volcaniclastic Rocks. Geological Society, London, Special Publications 16, 5–27.

Flower, M.F., Zhang, M., Chen, C.Y., Tu, K., Xie, G.H., 1992. Magmatism in the South China Basin 2. Post-spreading Quaternary basalts from Hainan Island, south China. Chemical Geology 97, 65–87.

Floyd, P.A., Winchester, J.A., 1975. Magma type and tectonic setting discrimination using immobile elements. Earth and Planetary Science Letters 27, 211–218.

Hall, R., 2002. Cenozoic geological and plate tectonic evolution of SE Asia and the SW Pacific: computer-based reconstructions, model and animations. Journal of Asian Earth Sciences 20, 353–431.

Hamelin, B., Allègre, C.J., 1985. Large scale regional units in the depleted upper mantle revealed by an isotopic study of the south-west Indian ridge. Nature 315, 196–198.

Hart, S.R., 1984. A large-scale isotope anomaly in the southern hemisphere mantle. Nature 309, 753–757.

Hart, S.R., Hauri, E.H., Oschmann, L.A., Whitehead, J.A., 1992. Mantle plumes and entrainment: isotopic evidence. Science 256, 517–520.

Ho, K.S., Chen, J.C., Lo, C.H., Zhao, H.L., 2003. ^{40}Ar–^{39}Ar dating and geochemical characteristics of late Cenozoic basaltic rocks from the Zhejiang–Fujian region, SE China: eruption ages, magma evolution and petrogenesis. Chemical Geology 197, 287–318.

Hoang, N., Flower, M., 1998. Petrogenesis of Cenozoic basalts from Vietnam: implication for origins of a 'diffuse igneous province'. Journal of Petrology 39, 369–395.

Hoang, N., Flower, M., Carlson, R., 1996. Major, trace element, and isotopic compositions of Vietnamese basalts: interaction of hydrous EM1-rich asthenosphere with thinned Eurasian lithosphere. Geochimica et Cosmochimica Acta 60, 4329–4351.

Hofmann, A.W., 1988. Chemical differentiation of the Earth: the relationship between mantle, continental crust and oceanic crust. Earth and Planetary Science Letters 90, 297–314.

Hsu, S.-K., Yeh, Y.-C., Doo, W.-B., Tsai, C.-H., 2004. New bathymetry and magnetic lineations identifications in the northernmost South China Sea and their tectonic implications. Marine Geophysical Research 25, 29–44.

Ishizuka, O., Yuasa, M., Taylor, R.N., Sakamoto, I., 2009. Two contrasting magmatic types coexist after the cessation of back-arc spreading. Chemical Geology 266, 274–296.

Janney, P.E., Castillo, P.R., 1996. Basalts from the Central Pacific Basin: evidence for the origin of Cretaceous igneous complexes in the Jurassic western Pacific. Journal of Geophysical Research 101 (B2), 2875–2893.

Kaneoka, I., Notsu, K., Takigami, Y., Fujioka, K., Sakai, H., 1990. Constraints on the evolution of the Japan Sea based on ^{40}Ar–^{39}Ar ages and Sr isotopic ratios for volcanic rocks of the Yamato Seamount chain in the Japan Sea. Earth and Planetary Science Letters 97, 211–225.

Karig, D.E., 1971. Origin and development of marginal basins in the Western Pacific. Journal of Geophysical Research 76 (11), 2542–2561.

Kincaid, C., Ito, G., Gable, C., 1995. Laboratory investigation of the interaction of off-axis mantle plumes and spreading centers. Nature 376, 758–761.

Klein, G., Kobayashi, K., Chamley, H., Curtis, D., Dick, H., Echols, D., Fountain, D., Kinoshita, H., Marsh, N., Mizuno, A., Nisterenko, G., Okada, H., Sloan, J., Waples, D., White, S., 1978. Off-ridge volcanism and seafloor spreading in the Shikoku Basin. Nature 273, 746–748.

Kudrass, H.R., Wiedicke, M., Cepek, P., Kreuzer, H., Muller, P., 1986. Mesozoic and Cenozoic rocks dredged from the South China Sea (Reed Bank area) and Sulu Sea and their significance for plate-tectonic reconstructions. Marine and Petroleum Geology 3, 9–30.

Lebedev, S., Nolet, G., 2003. Upper mantle beneath Southeast Asia from S velocity tomography. Journal of Geophysical Research 108 (B1), 20–48.

Lee, T.Y., Lo, C.H., Chung, S.L., Chen, C.Y., Wang, P.L., Nguyen, H., Cumg, T.C., Nguyen, T.Y., 1998. $^{40}Ar/^{39}Ar$ dating result of Neogene basalts in Vietnam and its tectonic implication. In: Flower, M.F.J., Chung, S.L., Lo, C.-H., Lee, T.-Y. (Eds.), Mantle Dynamics and Plate Interactions in east Asia. American Geophysical Union, Geodynamic series 27, pp. 317–330.

Lei, J., Zhao, D., Steinberger, B., Wud, B., Shene, F., Li, Z., 2009. New seismic constraints on the upper mantle structure of the Hainan plume. Physics of the Earth and Planetary Interiors 173, 33–50.

Lugmair, G.W., Galer, S.J., 1992. Age and isotopic relationships among the angfites Lewis Cliff 86010 and Angra dos Reis. Geochimica et Cosmochimica Acta 56, 1673–1694.

Mahoney, J.J., Natland, J.H., White, W.M., Poreda, R., Bloomer, S.H., Fisher, R.L., Baxter, A.N., 1989. Isotopic and geochemical provinces of western Indian Ocean spreading centers. Journal of Geophysical Research 94, 4033–4052.

McBirney, A.R., Murase, T., 1970. Factors governing the formation of pyroclastic Rocks. Bulletin of Volcanology 34 (2), 372–384.

Montelli, R., Nolet, G., Dahlen, F.A., Masters, M., 2006. A catalogue of deep mantle plumes: new results from finite frequency tomography. Geochemistry, Geophysics, Geosystems 7, Q11007. http://dx.doi.org/10.1029/2006GC001248.

Niu, Y., O'Hara, M., 2003. Origin of ocean island basalts: a new perspective from petrology, geochemistry, and mineral physics considerations. Journal of Geophysical Research 108 (B4), 2209. http://dx.doi.org/10.1029/2002JB002048.

Pouclet, A., Lee, J.-S., Vidal, P., Cousens, B., Bellon, H., 1995. Cretaceous to Cenozoic volcanism in South Korea and in the Sea of Japan: magmatic constraints on the opening of the back-arc basin. In: Smellie, J.L. (Ed.), Volcanism Associated with Extension at Consuming Plate Margins. Geological Society Special Publication 81, pp. 169–191.

Pritchard, M.E., Simons, M., 2002. A satellite geodetic survey of large-scale deformation of volcanic centres in the central Andes. Nature 418, 167–171.

Shi, X., Yan, Q., 2011. Geochemistry of Cenozoic magmatism in the South China Sea and its tectonic implications. Marine Geology & Quaternary Geology 31 (2), 59–72 (in Chinese with English abstract).
Straub, S.M., Goldstein, S.L., Class, C., Schmidt, A., 2009. Mid-ocean-ridge basalt of Indian type in the northwest Pacific Ocean basin. Nature Geosciences 2, 286–289.
Sun, S.S., McDonough, W.F., 1989. Chemical and isotopic systematics of oceanic basalts: implications of mantle composition and processes. Geological Society, London, Special Publications 42, 313–345.
Tapponnier, P., 1986. On the mechanics of the collision between India and Asia. Geological Society Special Publication 19, 115–157.
Tu, K., Flower, M.F.J., Carlson, R.W., Zhang, M., Xie, G., 1991. Sr, Nd, and Pb isotopic compositions of Hainan basalts (south China): implications for a subcontinental lithosphere Dupal source. Geology 19, 567–569.
Tu, K., Flower, M.F.J., Carlson, R.W., Xie, G., Chen, C.-Y., Zhang, M., 1992. Magmatism in the South China Basin 1. Isotopic and trace-element evidence for an endogenous Dupal mantle component. Chemical Geology 97, 47–63.
Wang, X.J., Wu, M.Q., Liang, D.H., Yin, A.W., 1984. Some geochemical characteristics of basalts from the South China Sea. Geochemica 4, 332–340 (in Chinese with English abstract).
Wang, K.L., Chung, S.L., Lo, Y.M., Lo, C.H., Yang, H.J., Shinjo, R., Lee, T.Y., Wu, J.C., Huang, S.T., 2012. Age and geochemical characteristics of Paleogene basalts drilled from western Taiwan: records of initial rifting at the southeastern Eurasian continental margin. Lithos 155, 426–441.
Wang, X.-C., Li, X.-H., Li, J., Liu, Y., Long, W.G., Zhou, J.B., Wang, F.T., Journal of Petrology, 2012. Temperature, pressure, and composition of the mantle source region of Late Cenozoic basalts in Hainan Island, SE Asia: a consequence of a young thermal mantle plume close to subduction zones? Journal of Petrology 53, 177–233.
Winchester, J.A., Floyd, P.A., 1977. Geochemical discrimination of different magma series and their differentiation products using immobile elements. Chemical Geology 20, 325–343.
Workman, R.K., Hart, S.R., 2005. Major and trace element composition of the depleted MORB mantle (DMM). Earth and Planetary Science Letters 231, 53–72.
Xu, Y., Wei, J., Qiu, H., Zhang, H., Huang, X., 2012. Opening and evolution of the South China Sea constrained by studies on volcanic rocks: preliminary results and a research design. Chinese Science Bulletin 57, 3150–3164.
Yan, Q., Shi, X., 2009. Characteristics of volcaniclastic rocks from seamounts in the South China Sea and its geological implications. Acta Petrologica Sinica 25, 3327–3334 (in Chinese with English abstract).
Yan, Q., Shi, X., Wang, K., Bu, W., Xiao, L., 2008a. Major element, trace element, Sr–Nd–Pb isotopic studies of Cenozoic alkali basalts from the South China Sea. Science in China, Series D: Earth Sciences 51 (4), 550–566.
Yan, Q., Shi, X., Yang, Y., Wang, K., 2008b. K–Ar/Ar–Ar geochronology of Cenozoic alkali basalts from the South China Sea. Acta Oceanologica Sinica 27 (6), 115–123.
Yan, Q., Shi, X., Castillo, P., 2014. The late Mesozoic–Cenozoic tectonic evolution of the South China Sea: a petrologic perspective. Journal of Asian Earth Sciences 85, 178–201.
Zhao, D., 2007. Seismic images under 60 hotspots: search for mantle plumes. Gondwana Research 12, 335–355.
Zhou, P.B., Mukasa, S.B., 1997. Nb–Sr–Pb isotopic, and major- and trace-element geochemistry of Cenozoic lavas from the Khorat Plateau, Thailand: sources and petrogenesis. Chemical Geology 137, 175–193.
Zhou, H., Xiao, L., Dong, Y., Wang, C., Wang, F., Ni, P., 2009. Geochemical and geochronological study of the Sanshui basin bimodal volcanic rock suite, China: implications for basin dynamics in southeastern China. Journal of Asian Earth Sciences 34, 178–189.
Zindler, A., Hart, S.R., 1986. Chemical geodynamics. Annual Review of Earth and Planetary Science Letters 14, 493–571.
Zou, H.B., Fan, Q.C., 2010. U–Th isotopes in Hainan basalts: implications for sub-asthenospheric origin of EM2 mantle endmember and the dynamics of melting beneath Hainan Island. Lithos 116, 145–152.
Zou, H.P., Li, P.L., Rao, C.T., 1995. Geochemistry of Cenozoic volcanic rocks in Zhujiangkou Basin and its geodynamic significance. Geochemica 24, 33–45 (Suppl., in Chinese with English abstrac0074).
Zou, H., Zindler, A., Xu, X., Qi, Q., 2000. Major, trace element, and Nd, Sr and Pb isotope studies of Cenozoic basalts in SE China: mantle sources, regional variations, and tectonic significance. Chemical Geology 171, 33–47.
Zou, H., McKeegan, K., Xu, X., Zindler, A., 2004. Fe–Al-rich tridymite–hercynite xenoliths with positive cerium anomalies: preserved lateritic paleosols and implications for Miocene climate. Chemical Geology 207, 101–116.